Journal of proteome research

Article

pubs.acs.org/jpr

Integrative Analysis of Transcriptomics, Proteomics, and Metabolomics Data of White Adipose and Liver Tissue of High-Fat Diet and Rosiglitazone-Treated Insulin-Resistant Mice Identified Pathway Alterations and Molecular Hubs

David Meierhofer, Christopher Weidner, and Sascha Sauer*

Max Planck Institute for Molecular Genetics, Ihnestraße 63-73, 14195 Berlin, Germany

Supporting Information

ABSTRACT: The incidences of obesity and type 2 diabetes are rapidly increasing and have evolved into a global epidemic. In this study, we analyzed the molecular effects of high-fat diet (HFD)-induced insulin-resistance on mice in two metabolic target tissues, the white adipose tissue (WAT) and the liver. Additionally, we analyzed the effects of drug treatment using the specific PPARγ ligand rosiglitazone. We integrated transcriptome, proteome, and metabolome data sets for a combined holistic view of molecular mechanisms in type 2 diabetes. Using network and pathway analyses, we identified hub proteins such as SDHB and SUCLG1 in WAT and deregulation of major metabolic pathways in the insulin-resistant state, including the TCA cycle, oxidative phosphorylation, and branched chain amino acid metabolism. Rosiglitazone treatment resulted mainly in modulation via PPAR signaling and oxidative phosphorylation in WAT only. Interestingly, in HFD liver, we could observe a decrease of proteins involved in vitamin B metabolism such as PDXDC1 and DHFR and the according metabolites. Furthermore, we could identify sphingosine (Sph) and sphingosine 1-phosphate (SP1) as a drug-specific marker pair in the liver. In summary, our data indicate physiological plasticity gained by interconnected molecular pathways to counteract metabolic dysregulation due to high calorie intake and drug treatment.

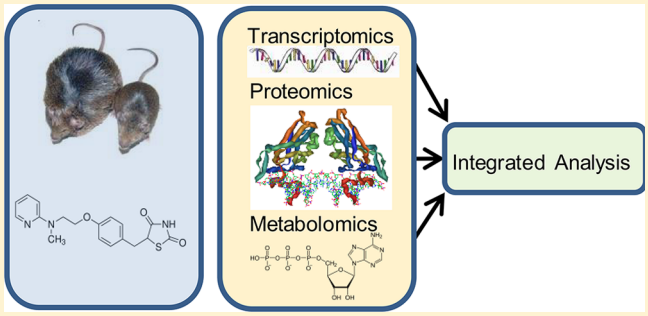

KEYWORDS: *type 2 diabetes, obesity, mass spectrometry, molecular pathways, biomarkers, network analysis*

INTRODUCTION

Metabolic disorders such as obesity and type 2 diabetes are a major current health problem, in particular in countries of growing economic power, along with significant lifestyle changes such as low physical activity and high-calorie intake.[1] Researchers have been extensively studying the etiology and molecular mechanisms of these disorders to gain basic insights and develop treatment strategies. However, physiological alterations resulting from environmental changes such as high calorie intake do not affect only a few key proteins or other functionally important biomolecules. Instead, homeostasis is secured by the robustness of molecular networks.[2,3] It is thus conceivable that identification of deregulated pathways and networks is a fruitful discovery approach, as a starting point for later analyses of molecular mechanisms and validation of potential disease biomarkers.

The initial proteomic-based studies in the diabetes research field have included proteomic studies of pancreatic islets in animal models of obesity and diabetes,[4] diabetic nephropathy,[5] pancreas from pancreatectomy models,[6] fat,[7] muscle,[8] and liver.[9,10] Results of such studies were usually limited to short lists of regulated proteins.

Furthermore, recent metabolite studies in blood, plasma, or serum indicated potential physiological deregulation in diabetic mice and patients.[11,12] Recently, combined RNA expression and metabolite analyses were shown for diabetic mouse models,[13] but these studies could not systematically decipher potential impact of the most functionally relevant proteins.

Recently, we started analyses in various diabetic mouse models,[14,15] introducing the concept of protein sets for providing diagnostic tools for preclinical drug development.[16] In this study, we primarily aimed to gain a holistic view on the physiological deregulation in a high-fat diet (HFD)-induced insulin-resistance mouse model. Therefore, we used comprehensive data sets of transcripts, proteins, and metabolites derived from two major metabolic target tissues, the white adipose tissue (WAT) and the liver. We further aimed to analyze the effects of the diabetes drug rosiglitazone (RGZ), a thiazolidinedione which specifically targets the peroxisome proliferator-activated receptor gamma (PPARγ).[17] The nuclear receptor PPARγ is highly abundant in WAT, suggesting that the insulin-sensitizing effects of RGZ are mainly driven by

Received: June 13, 2014

   dx.doi.org/10.1021/pr5005828 | J. Proteome Res. XXXX, XXX, XXX−XXX

physiological effects derived from fat tissue,[18] whereas PPARγ is less abundant in liver.

Therefore, we analyzed WAT and liver tissue on a global scale in terms of (i) the relative expression levels of coding transcripts based on microarray analyses, (ii) the relative expression levels of proteins based on shotgun LC-MS/MS using a SILAC mouse approach with $^{13}C_6$-lysine-labeled reference tissues, and (iii) the relative metabolite abundances based on targeted LC-MS/MS technology. All data were derived from the same mouse cohorts.

EXPERIMENTAL PROCEDURES

Mouse Samples

Animal studies were carried out according to internationally approved standards, as described recently,[15,16] and have been validated and approved by the State Office of Health and Social Affairs, Berlin (LAGeSo). As stated previously "the animals were maintained one per cage under temperature-, humidity-, and light-controlled conditions (22°C, 50% humidity, 12 h light/12 h dark cycle). The health status and behaviour of mice were examined daily. Mice had ad libitum access to food and water. Mice and food were weighed regularly to determine changes in body weight and food intake. Low-fat diet (LFD, D12450B, 10 kcal% fat, 18.0 MJ/kg, ssniff, Soest, Germany) was composed of the following: 4.1% crude fat, 18.1% crude protein, 26.6% starch, 35.5% sugar/dextrines, 4.7% crude fiber. High-fat diet (HFD, D12492, 60 kcal% fat, 25.3 MJ/kg, ssniff) was composed of the following: 34.0% crude fat, 24.1% crude protein, 1.1% starch, 23.8% sugar/dextrines, 6.0% crude fiber.[16]

Six-week-old male C57BL/6 mice were fed a high-fat diet (HFD) for 12 weeks to generate insulin-resistant diet-induced obesity (DIO) mice. Then, the mice were weighed and equally distributed to two groups (n = 13 each). DIO mice were treated over 3 weeks with 4 mg/kg/d RGZ or vehicle only. Mice of similar age fed with low-fat diet (LFD) were considered as healthy controls. Liver and visceral white adipose tissue were dissected, washed in phosphate-buffered saline (PBS, pH7.4), and shock frozen in liquid nitrogen. Plasma and tissues were stored at −80 °C before use.

To document HFD-induced insulin resistance and the physiological effects of RGZ treatment in all mice, we determined the fasted levels of glucose, insulin, triglycerides, and free fatty acids in plasma, using standard procedures.[14] Homeostasis model assessment of insulin resistance (HOMA-IR) was determined as follows: fasting glucose (mg/dL) × fasting insulin (μU/mL)/405.[19]

Gene Expression Analysis

Genome-wide RNA expression analysis was done using standard procedures including Illumina sample preparation protocols and the Illumina BeadStation 500 platform as described recently.[16] Integrity of RNA was checked by use of standard agarose gel electrophoresis and ethidium bromide staining. Samples from randomly chosen mice of a treatment cohort were analyzed using at least biological triplicates. Basic expression data analyses were performed using GenomeStudio V2011.1 (Illumina). Raw data were background-subtracted and normalized applying the cubic spline algorithm. Processed data were subsequently filtered for significant detection (P value ≤0.01) and differential expression vs vehicle treatment according to the Illumina t test error model, and were corrected according to the Benjamini−Hochberg method (P value ≤0.05) of the GenomeStudio software. Gene expression data were submitted in MIAME-compliant form to the NCBI Gene Expression Omnibus database (GSE38856). All double log blots were made in Perseus v.1.4.0.8.[20] For consistency, all gene and protein information was retrieved from the UniProtKB (www.uniprot.org, April 2014).

Protein Expression Analysis

Protein data analysis was based on a previous study published by us.[16] In brief, to cope with large variability of protein expression comparted to RNA expression in animal tissues, pools from eight randomly chosen mice per cohort were sampled in frozen condition, as described recently.[16] A lysis buffer containing 4% SDS, 0.1 M DTT, 0.1 M Tris pH 8.0 was added. SILAC mouse reference tissues ($^{13}C_6$-lysine-labeled reference tissues (Silantes, Martinsried, Germany)) were lysed in the same way. For protein separation, samples were mixed 1:1 with the SILAC reference samples. About 200 μg of protein was loaded onto a 12% SDS gel, and 18 fractions were Lys-C digested. Each sample was dissolved in 5% ACN, 2% FA and were used for LC-MS analysis.

Nano liquid chromatography (LC), online coupled to a Linear Ion Trap (LTQ)-Orbitrap XL mass spectrometer (Thermo-Electron Corp) was used to sequence peptides eluting from a PicoFrit analytical column (75 μm ID × 150 mm long, 15 μm Tip ID (New Objectives, Woburn, MA)) in-house packed with 3 μm C18 resin (Reprosil-AQ Pur, Dr. Maisch, Germany). A nonlinear gradient from 2 to 40% solvent B over 160 min at a flow rate of 200 nL/min (solvent A: 97.9% H_2O, 2% acetonitrile, 0.1% formic acid; solvent B: 97.9% acetonitrile, 2% H_2O, 0.1% formic acid) was used. A voltage of 1.8 kV was applied for nanoelectrospray generation. A cycle of one full FT scan mass spectrum (300−2000 m/z, resolution of 60 000 at m/z 400) was followed by 10 data-dependent MS/MS scans acquired in the linear ion trap with normalized collision energy (setting at 35%). Target ions already selected for MS/MS were dynamically excluded for 60 s. Raw files for each LC−MS/MS experiment were submitted to MaxQuant v1.0.13.13 for data processing. The cutoff value was set to 1% FDR. As SILAC modification, we used $^{13}C_6$-labeled lysine. The following chemical modifications were selected as variable modifications: protein N-terminal acetylation and methionine oxidation. Carbamidomethyl C was used as fixed modification. Lys-C was set with a maximum of two missed cleavage sites. Mass tolerance for precursor and fragment ions was 0.5 Da and 7 ppm. Sample pools were run as technical replicates, respectively. Raw- and MaxQuant processed mass spectrometry data that were used in this study can be downloaded via: ftp://PASS00201:BG7335ub@ftp.peptideatlas.org/.

As desribed recently,[16] protein expression changes between samples were calculated using the formula below:

$$\frac{\dfrac{^{12}C_6\ \text{condition 1}}{^{13}C_6\ \text{reference}}}{\dfrac{^{12}C_6\ \text{condition 2}}{^{13}C_6\ \text{reference}}} = \frac{^{12}C_6\ \text{condition 1}}{^{12}C_6\ \text{condition 2}}$$

Metabolite Extraction

Metabolite analysis was done with the same tissue samples as for protein expression analysis (see above). Tissues were dissected, washed in phosphate-buffered saline (PBS, pH7.4), and shock frozen in liquid nitrogen. To enable discovery of reliable changes in metabolome states in visceral adipose and

dx.doi.org/10.1021/pr5005828 | J. Proteome Res. XXXX, XXX, XXX−XXX

liver tissue, we used pools from eight randomly chosen mice (100−160 mg in total) per treatment cohort. The final ratio of solvents used in the biphasic methanol/chloroform/water extraction method was 2.0/2.0/1.8.[21] Cold methanol (500 μL, −20 °C) and 107 μL of water were added to the frozen tissue pools and subsequently homogenized by FastPrep (settings: 2 × 40 s; 4.5 m/s) with a steel ball. Samples were kept on ice, and 250 μL of chloroform was added to the homogenate. Appropriate safety guidelines have to be put in place while working with chloroform. Samples were vortexed for 10 min and centrifuged for 5 min at 2000*g* at 4 °C to remove debris and precipitated protein. The supernatant was transferred to a new tube, and 250 μL of chloroform and 250 μL of water were added. Samples were again vortexed for 60 s, kept on ice for 10 min for phase separation, and centrifuged for 10 min at 2000*g* at 4 °C. Resulting upper polar and lower nonpolar fractions were separately transferred and combined in three clean tubes containing the internal standard chloramphenicol, dedicated for subsequent analysis by using methanol, acetonitrile, and water as alternative solvents for LC-MS runs. Samples were lyophilized in the centrifugal concentrator.

Targeted LC-MS/MS Analysis of Metabolites

We applied a multi reaction monitoring (MRM)-based strategy to identify differences in metabolite abundance of sample cohorts. The residuals from the previous step were suspended in 35 μL of acetonitrile, 0.1% formic acid and 35 μL of methanol, 0.1% formic acid for analysis by HILIC mode and in 20 μL of water, 0.1% formic acid for RPLC mode. Samples were centrifuged at 17 500*g* for 5 min at 4 °C. Samples were further cleaned to avoid column clogging (iso-disc filters PTFE 13 mm × 0.2 mm, Supelco, Bellafonte, PA). The supernatants were transferred to microvolume inserts, and 5 μL per run was injected for LC-MS/MS analysis. The sample pools were run as technical triplicates.

Metabolites were analyzed using an online coupled LC-MS/MS system (1290 Infinity UHPLC, Agilent, Santa Clara, CA; QTrap 6500, ABSciex, Toronto, Canada) featuring a Reprosil-PUR C18-AQ (1.9 μm, 120 Å, 150 × 2 mm ID; Dr. Maisch; Ammerbuch, Germany) column and a zicHILIC (3.5 μm, 100 Å, 150 × 2.1 mm ID; di2chrom; Marl, Germany) column at controlled temperature of 30 °C. The chromatographic separations were performed on RP and zicHILIC stationary phases. The UHPLC was run with four different buffer conditions: A1:10 mM ammonium acetate in LC-MS grade water (adjusted with formic acid to pH 3.5); A2:10 mM ammonium acetate in LC-MS grade water (adjusted with ammonium hydroxide to pH 7.5); B1: LC-MS grade acetonitrile; 0.1% FA; B2: LC-MS grade methanol; 0.1% formic acid. Gradients and flow conditions are described in Supporting Information, Table 1. The columns were equilibrated with a blank run in the according buffer system, and in the case of methanol methods, three blank runs were necessary for a proper equilibration.

MS-Data acquisition was performed with an ion spray voltage of 5.5 kV in positive mode and 4.5 kV in negative mode of the ESI source. Nitrogen as collision gas was set to high, curtain gas to 30 psi, ion source gas 1 and 2 to 50 and 70 psi, respectively, and an interface heater temperature of 350 °C was used. The mass spectrometer was operated with AB Sciex Analyst 1.6.1 software with components for 6500 series instruments.

Transitions were monitored and acquired at unit resolution (peak width at 50% was 0.7 Da ± 0.1 Da tolerance) in quadrupole Q1 and Q3. At least two transitions per metabolite were monitored in this MRM based method. The scheduled MRM algorithm, monitoring transitions only 300 s around the expected retention time, was used to decrease the number of concurrent MRMs monitored at any time point.

Metabolite MS Data Integration

Compound quantification was performed using MultiQuant software v.2.1.1 (AB Sciex, Foster City, CA). Integration settings were a Gaussian smooth width of 2 points and a peak splitting factor of 2. Peak integrations were reviewed manually, and results tables were exported as Excel files. Metabolite identification was based on co-occurring transitions at the expected retention time and at least 10 times smaller peak areas in blank runs. An additional feature used to correctly identify analytes was the ratio between the transitions, which had to match the ratios of the according tuned pure metabolites. Samples were normalized according to the weight of used tissue per cohort. The average ratio from all MRMs of one metabolite was used to calculate the log fold change between sample cohorts. Perseus v.1.4.0.8 was used for generating density scatter blots.

Gene/Protein Set Enrichment, Network, and Pathway Analyses

We used the Gene Set Enrichment Analysis (GSEA) tool,[22] v2.0.14 (http://www.broadinstitute.org/gsea/index.jsp) to analyze whether an a priori defined set of genes or proteins revealed statistical significance and concordant differences between two biological states. In general, the following parameters were chosen if not otherwise noted: 10 000 gene/protein set permutations, weighted enrichment statistics, minimal gene/protein set size of 5, and log2 ratio metric with preranking. RNA expression data and protein SILAC ratios were analyzed using the KEGG database (version 4.0, 186 pathways) from the Molecular Signature Database (MSigDB). We considered regulated pathways only as statistically significant, if the FDR was ≤0.25. Heatmaps were carried out with Mayday 2.13.[23] Qualitative correlation was determined as the part of the genes that were regulated in a similar direction by RNA and protein expression. A correlation of 50% was considered as random. For correlation analyses on the single gene/protein level, genes and proteins were filtered for candidates with fold change ≥1.33 or ≤0.75 for RNA or protein. For correlation analyses on pathway levels, we compared the KEGG pathway regulation determined by GSEA, and we included only regulated pathways with FDR ≤ 0.25 for RNA or protein. Correlation analyses were done separately for each treatment and tissue.

To identify the main hub proteins, we generated interaction networks using STRING 9.1.[24] We applyed a high confidence score of 0.7, which implies that only interactions with a high level of confidence were extracted from the database and considered as valid links for protein−protein interaction (PPI) networks.

Interaction networks were extracted and further analyzed and evaluated using the Cytoscape v3.1.1[25] plugin called "network analyzer".[26] Network analyzer was used to identify hub proteins, carrying the highest closeness centrality (CC), betweenness centrality (BC), and the node degree as key topological parameters.[27] Network robustness was measured as an iterative resilience in terms of removal of nodes. KEGG pathways were used to visualize pathways within the networks, and unconnected nodes were removed.

dx.doi.org/10.1021/pr5005828 | J. Proteome Res. XXXX, XXX, XXX−XXX

For integrated pathway analyses of gene/protein expression and metabolomics data, we applied Integrated Molecular Pathway Level Analysis (IMPaLA).[28]

RESULTS AND DISCUSSION

The development of diet-induced insulin resistance and treatment thereof involves complex physiological processes.

Table 1. Analyzed Physiological Parameters of LFD-Fed, HFD-Fed, and RGZ-Treated HFD-Fed Mice

parameter	LFD	HFD	HFD + RGZ
body weight (g)	28.1 ± 1.5	41.7 ± 2.3	42.5 ± 4.4
plasma glucose (mM)	4.8 ± 1.0	7.2 ± 1.3	6.3 ± 1.0
plasma insulin (ng/mL)	0.7 ± 0.2	1.3 ± 0.3	0.8 ± 0.4
HOMA-IR	3.5 ± 0.9	10.9 ± 3.0	5.7 ± 3.9
plasma triglycerides (mM)	0.6 ± 0.1	1.8 ± 0.3	1.3 ± 0.2
plasma free fatty acids (mM)	0.4 ± 0.2	0.5 ± 0.1	0.3 ± 0.1

To investigate molecular aspects of these perturbations in WAT and liver, we fed mice either with a LFD or HFD to induce overweight and insulin resistance. We further treated insulin-resistant HFD-fed mice with the antidiabetic drug rosiglitazone to achieve insulin-sensitizing and lipid-lowering effects. Basic physiological parameters such as body weight, plasma glucose, insulin, triglycerides, free fatty acids, and homeostatic model assessment of insulin resistance (HOMA-IR) index confirmed diet-induced obesity and insulin resistance, as well as physiological effects of rosiglitazone drug treatment are summarized in Table 1.

Regulation of Molecules on the Transcriptome, Proteome, and Metabolome Level in White Adipose Tissue and Liver

Using microarray-based RNA expression analysis, we detected about 10 000 expressed genes in WAT and liver tissues. Strikingly regulated transcripts between LFD, HFD, and RGZ treatment are indicated in Figure 1A for WAT and Figure 1B for liver tissue. These transcripts can be attributed to various cellular functions such as inflammation or fatty acid metabolism.

More background information on the biological context of the most interesting regulated transcripts is provided in the Supporting Information. The highlighted gene transcripts may serve as a starting point for further mechanistic analysis and potentially represent candidates for biomarker development. For further holistic analysis, we considered the full data set displayed in Figure 1 to extract biological pathway information (see below).

In the proteomics data sets, we then identified several thousand proteins of which one-quarter was ≥2-fold regulated in LFD versus HFD and only a fraction of 7% upon RZG treatment in WAT as well as liver tissue. As for the transcriptome data, we analogously analyzed protein expression changes in white adipose and liver tissue, and we identified strongly up and down regulated proteins resulting from the diseased HFD-state or intervention by RGZ-treatment (Figure 2). Notably, many of the highly regulated proteins could not be observed in the transcriptomics analysis, with few exceptions, suggesting differential regulation and life times of RNAs and proteins.

As shown in Figure 2A, the entire set of identified proteins showed higher alterations compared to the RNA expression data set in WAT. Up regulated proteins in HFD compared to the LFD condition were histone proteins such as HIST1H1A, HIST1H1B, and FBN1, a structural component of extracellular microfibrils. The most striking down regulated proteins in HFD compared to the LFD condition were the following: fatty acid binding protein 1 (FABP1); proteins involved in mitochondrial context such as HSD17B10, PHB, UQCRC1, ADH1, and TST; and also ACTA2 (alpha-actin 2), a protein rather known in the context of muscle, which may probably also be involved in the context of cell motility, structure, and integrity of adipocytes. Cytoskeleton rearrangements have been found previously in this context.[29] Proteins which were down regulated in HFD and up regulated by RGZ treatment were actin-binding proteins TAGLN and TAGLN2; EPHX2, involved in xenobiotic

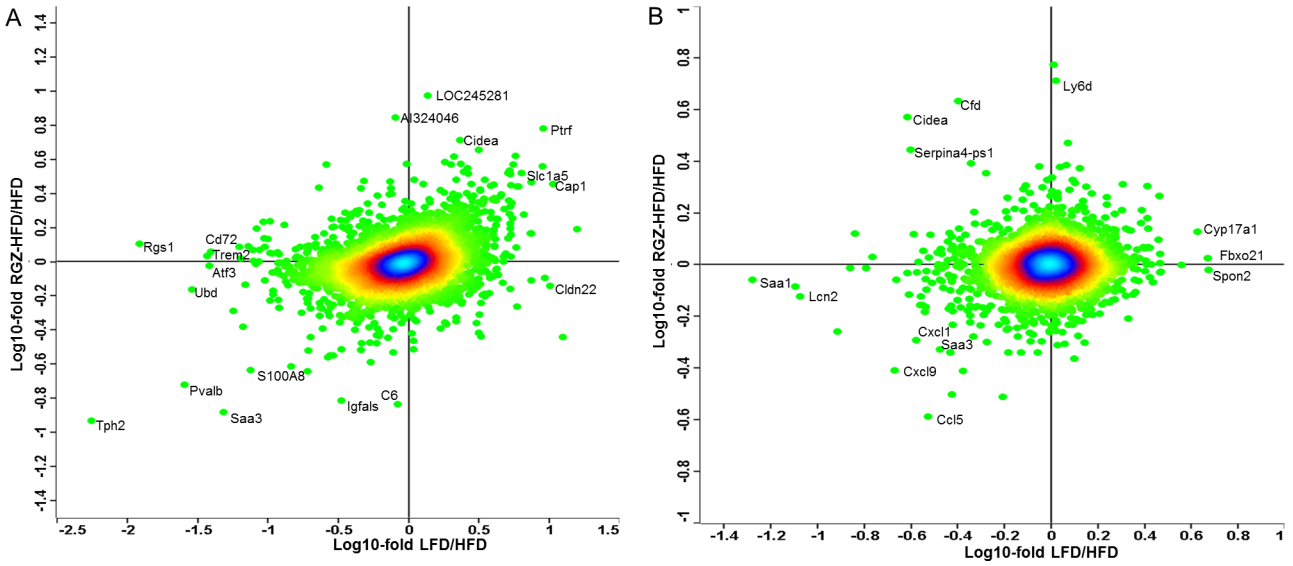

Figure 1. Log−log plot of the two conditions LFD/HFD and RGZ-HFD/HFD based on RNA expression ratios. (A) WAT, (B) liver tissue. The entire set of identified RNAs was distributed around the "unregulated" center. Strong gene expression changes are indicated, and biological background information is provided in the Supporting Information.

dx.doi.org/10.1021/pr5005828 | J. Proteome Res. XXXX, XXX, XXX−XXX

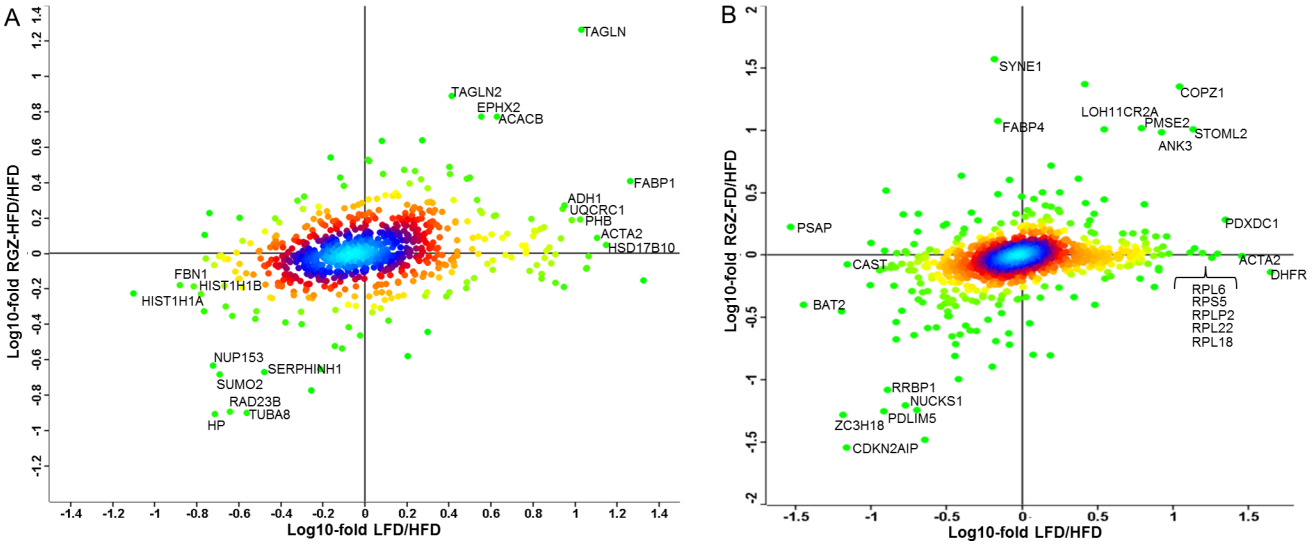

Figure 2. Log−log plot of the two conditions LFD/HFD and RGZ-HFD/HFD based on protein expression ratios. (A) WAT, (B) liver tissue. Outstanding protein expression changes are indicated according to their gene names. Biological background information for liver proteins is provided in the Supporting Information.

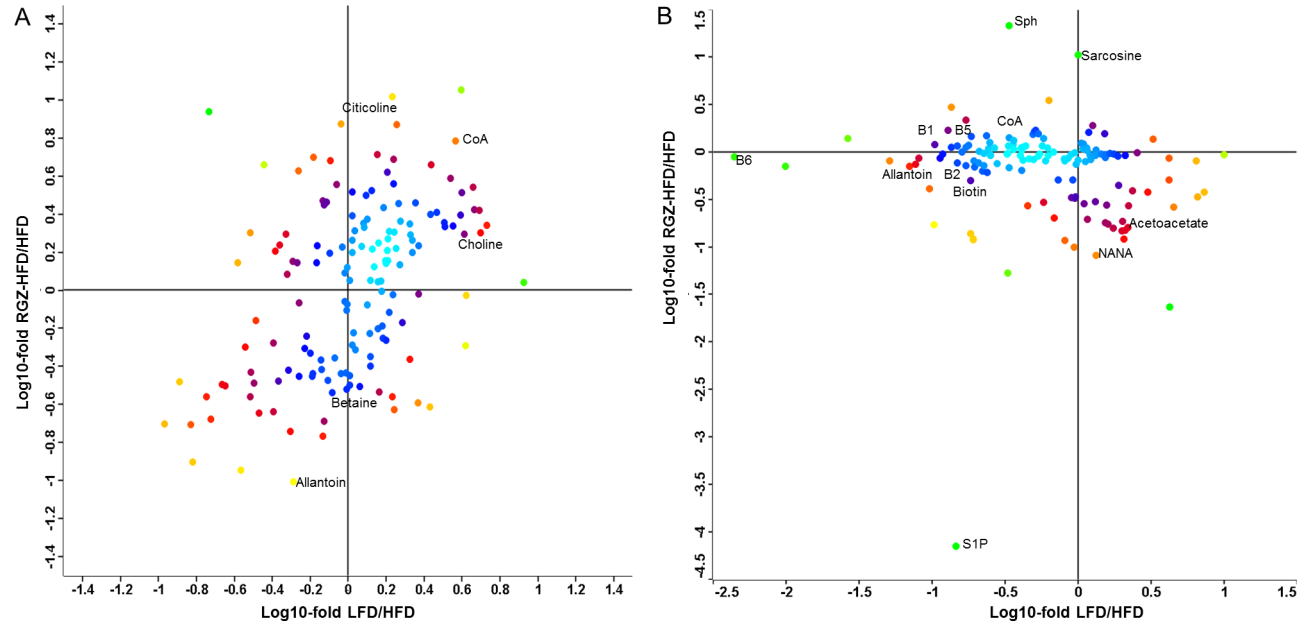

Figure 3. Log−log plot of the two conditions LFD/HFD and RGZ-HFD/HFD based on metabolite expression ratios. (A) WAT, (B) liver tissue.

metabolism of drugs; and ACACB, which may play a role in the regulation of fatty acid oxidation. Proteins that were down regulated in HFD and counteractively up regulated due to RGZ treatment were HP, haptoglobin, known to be involved in heme iron metabolism and also in the acute phase response, depending on the physiological context; proteins involved in cellular structure such as TUBA8, NUP153 and SERPINH1; and proteins involved in protein degradation such as RAD23B and SUMO2. Detailed information on the biological context of the highest regulated proteins in liver is given in the Supporting Information.

Finally, applying state-of-the-art targeted LC-MS/MS based metabolomics, we identified a set of 153 metabolites in WAT and 142 in liver tissue (Figure 3A,B, Supporting Information, Table 2). The entire set of identified metabolites was not at all distributed around the "unregulated" center like the transcriptome or proteome data. The metabolite data instead showed high variance and fold changes.

In WAT, coenzyme A (CoA), important for the metabolism of fatty acids and the oxidation of pyruvate in the citric acid cycle, was 3.7-fold down regulated in the HFD compared to the LFD state. Upon RGZ treatment, CoA amounts were even 2-fold higher than LFD levels, potentially re-establishing energy metabolism. Citicoline has been shown to restore the activity of mitochondrial ATPase and membrane Na+/K+ ATPase and has a neuroprotective effect in hypoxic and ischemic conditions.[30] Only in RGZ-treated WAT were we able to detect a 7.5-fold up regulation of citicoline, whereas this metabolite was unaffected in HFD versus LFD. This effect of RGZ could potentially contribute to restore the significantly deteriorated OXPHOS system in the HFD state, which was

dx.doi.org/10.1021/pr5005828 | J. Proteome Res. XXXX, XXX, XXX−XXX

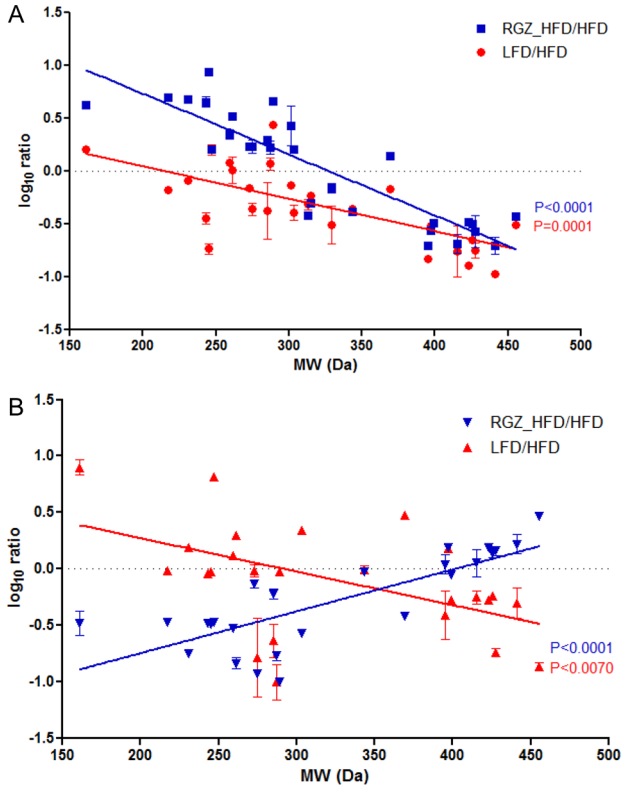

Figure 4. Acylcarnitines are presented according to their molecular masses on the X-axis against their log10 ratios of LFD/HFD and RGZ-HFD/HFD conditions in (A) WAT and (B) liver tissue. SD of MRMs, linear regression lines, and according p values are indicated.

corroborated by protein expression data showing increased expression of proteins involved in OXPHOS.

In liver, HFD compared to LFD state showed significant changes in metabolite levels. In contrast, RGZ treatment only showed marginal effects with few exceptions: The most interesting regulated metabolites in liver were the sphingolipids sphingosine (Sph) and sphingosine-1-phosphate (S1P). Sph usually inhibits proliferation and promotes apoptosis, while S1P stimulates tumor growth and suppresses apoptosis.[31] These metabolites are interconvertible; it is therefore believed that their relative ratio determines cell fate. As shown in Figure 3B, in liver tissue, the HFD/LFD ratio of Sph/S1P was 1:1. Strikingly, upon RGZ treatment, nearly 100% of S1P was converted to Sph, shifting the organ to a pro-apoptotic state, indicating potential hepatic toxicity of some thiazolidinediones, as recently reported.[32]

Another major regulated metabolite was *N*-acetylneuraminic acid (NANA, also known as sialic acid), which was increased in type 2 diabetes mellitus.[33] NANA levels were unchanged when HFD and LFD states were compared, but they decreased 12-fold upon RGZ treatment of HFD mice, confirming the insulin-sensitizing effects of RGZ.

In liver, allantoin was 20-fold elevated in the HFD state. However, in contrast to WAT, RGZ treatment could restore normal levels of allantoin, indicating metabolically beneficial effects.

All measured vitamin B metabolites (B1, B2, B5, B6, and biotin) were highly reduced in the HFD liver (6-fold in average) compared to LFD, and RGZ treatment could not restore these reduced metabolite levels (Figure 3B). This was consistent with the protein expression data, including strong down regulation of proteins involved in vitamin B metabolism (B6, folic acid), namely, PDXDC1 and DHFR. Furthermore, the dipeptide cystathionine was down regulated in HFD liver. Notably, excess levels of cystathionine in urine are an indicator of a prominent manifestation of vitamin-B6 deficiency called cystathioninuria.[34] Further research has to be done to elucidate the role of cystathionine in the context of liver and diabetes. The biological roles of further metabolites, which are not mentioned here, are described in Supporting Information.

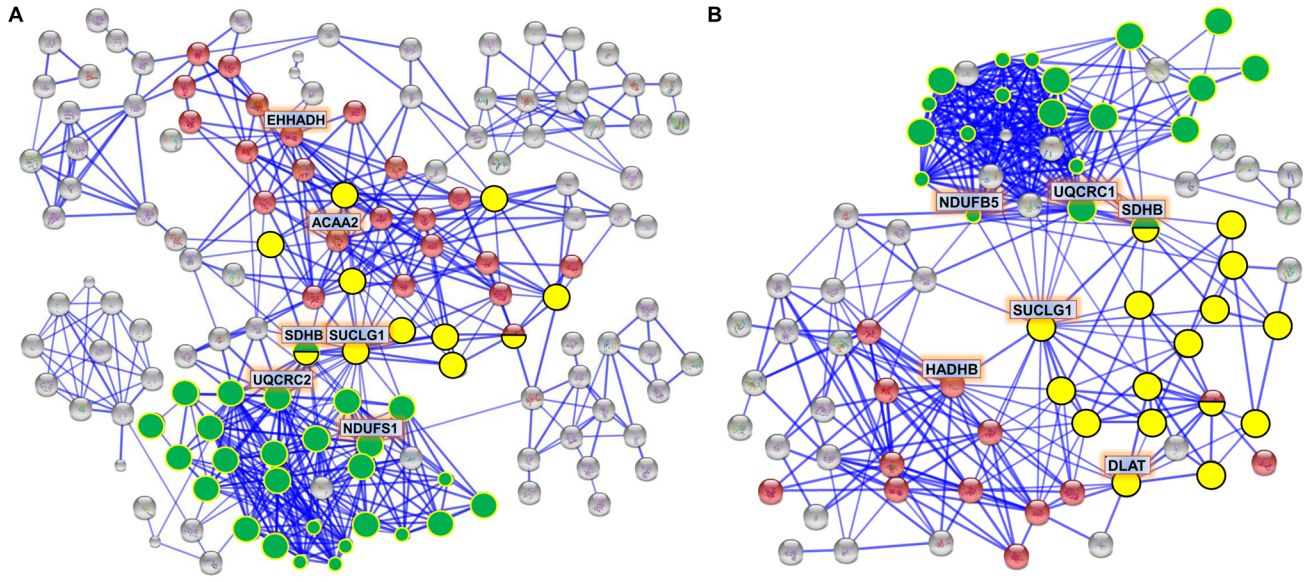

Figure 5. Network of down regulated proteins in (A) LFD/HFD and (B) RGZ-HFD/HFD fat tissue, visualized by STRING software (version 9.1). The top hub proteins are indicated according to Table 2. Proteins are colored according their KEGG pathway affiliation: red = BCAA, yellow = TCA cycle, and green = OXPHOS.

dx.doi.org/10.1021/pr5005828 | J. Proteome Res. XXXX, XXX, XXX−XXX

Table 2. Network Analysis of down Regulated LFD/HFD and RGZ-HFD/HFD Proteins in WAT To Determine the Main Hubs in Terms of Robustness and Betweenness Centrality

protein	nodes	average distance	network diameter	node degree	betweenness centrality	closeness centrality
network LFD/HFD down	165	4.49	12			
SDHB	164	4.66	12	20	0.21	0.34
SUCLG1	163	4.81	12	21	0.12	0.34
NDUFS1	158	6.82	19	16	0.11	0.32
EHHADH	154	7.48	21	18	0.08	0.27
ACAA2	152	7.87	21	18	0.05	0.32
UQCRC2	148	9.16	24	28	0.06	0.33
network RGZ/HFD down	108	2.83	8			
SUCLG1	107	2.98	8	21	0.27	0.52
UQCRC1	106	3.10	8	27	0.16	0.50
NDUFB5	105	3.38	9	23	0.06	0.48
SDHB	104	3.52	9	16	0.04	0.43
DLAT	102	4.05	11	12	0.05	0.38
HADHB	100	4.46	11	19	0.12	0.45

Nodes are connected proteins within a network; the average distance between nodes is calculated after removal of a node; the diameter of a network is defined as the longest of all calculated shortest paths in a network. All these three criteria are indicators of the network robustness and resilience. Node degree is the number of connections between one node to others; the betweenness centrality is equal to the number of shortest paths from all vertices to all others that pass through that node; closeness centrality is the distance metric between all nodes, defined by the length of their shortest paths.

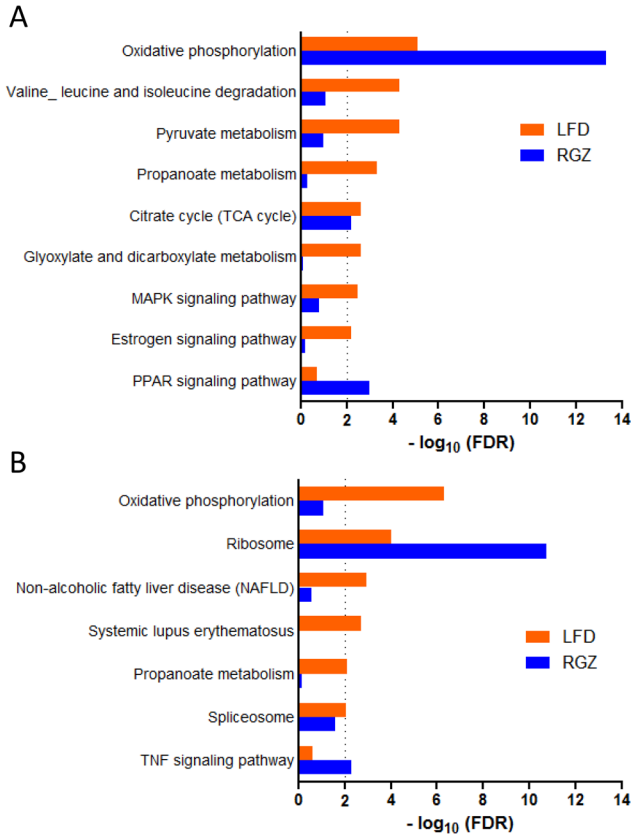

Figure 6. Visualization of selected significantly regulated KEGG pathways of RNA, protein, and metabolite data based on the pathway overrepresentation analysis. (A) WAT, (B) liver tissue.

Acylcarnitines: An Interesting Example of the Metabolite Data Sets

Carnitine and its acyl esters, the acylcarnitines, are essential compounds for the metabolism of fatty acids. As the acylation state of carnitine in the plasma reflects the composition of the cytosolic acylcarnitine pool, this serves as a diagnostic marker for the equilibrium between acyl-CoA and acylcarnitine species. For example, acylcarnitines generated as products of incomplete mitochondrial fatty acid oxidation have been detected in obesity, type 2 diabetes, cardiovascular disease, and encephalopathy and frequently lead to low levels of acetyl-CoA and dysfunction of the citric acid cycle.[35] Although most studies analyzed acylcarnitines in plasma, we focused on tissues.

Short acylcarnitines were down regulated in WAT-HFD state, whereas long acylcarnitines were up regulated, compared to both LFD and RGZ treatment (Figure 4A, Supporting Information, Table 3A). In liver, we observed similar regulation patterns for LFD versus HFD. However, for the RGZ treatment, we discovered an antiparallel regulation (Figure 4B, Supporting Information, Table 3B). Carnitine levels and short acylcarnitines were down regulated, but longer acylcarnitines were up regulated compared to HFD, suggesting a significant influence of RGZ on the fatty acid metabolism as energy source.

Others have found that short and long acylcarnitines can be differentially regulated in diabetes derived from plasma samples.[36−38] The reason remains speculative; however, it has been suggested that inefficient beta-oxidation of long-chain fatty acids, in part due to a relatively low citric acid cycle capacity, increases tissue accumulation of acetyl-CoA, which in turn generates chain-shortened acylcarnitines that trigger proinflammatory pathways involved in insulin resistance.[36] Our data seem to corroborate this hypothesis.

Holistic Views on Gene and Protein Expression and on Metabolomics Data

This is one of the first studies, which provides combined comprehensive "omics" data on three biological levels in a disease-relevant in vivo context. Figures 1−3 show that most of the transcripts were indeed unregulated, whereas the metabolome displayed a strong regulation. If we put these "optic impressions" into numbers (e.g., for LFD versus HFD liver), we find that the transcriptome ratios showed the smallest

dx.doi.org/10.1021/pr5005828 | J. Proteome Res. XXXX, XXX, XXX−XXX

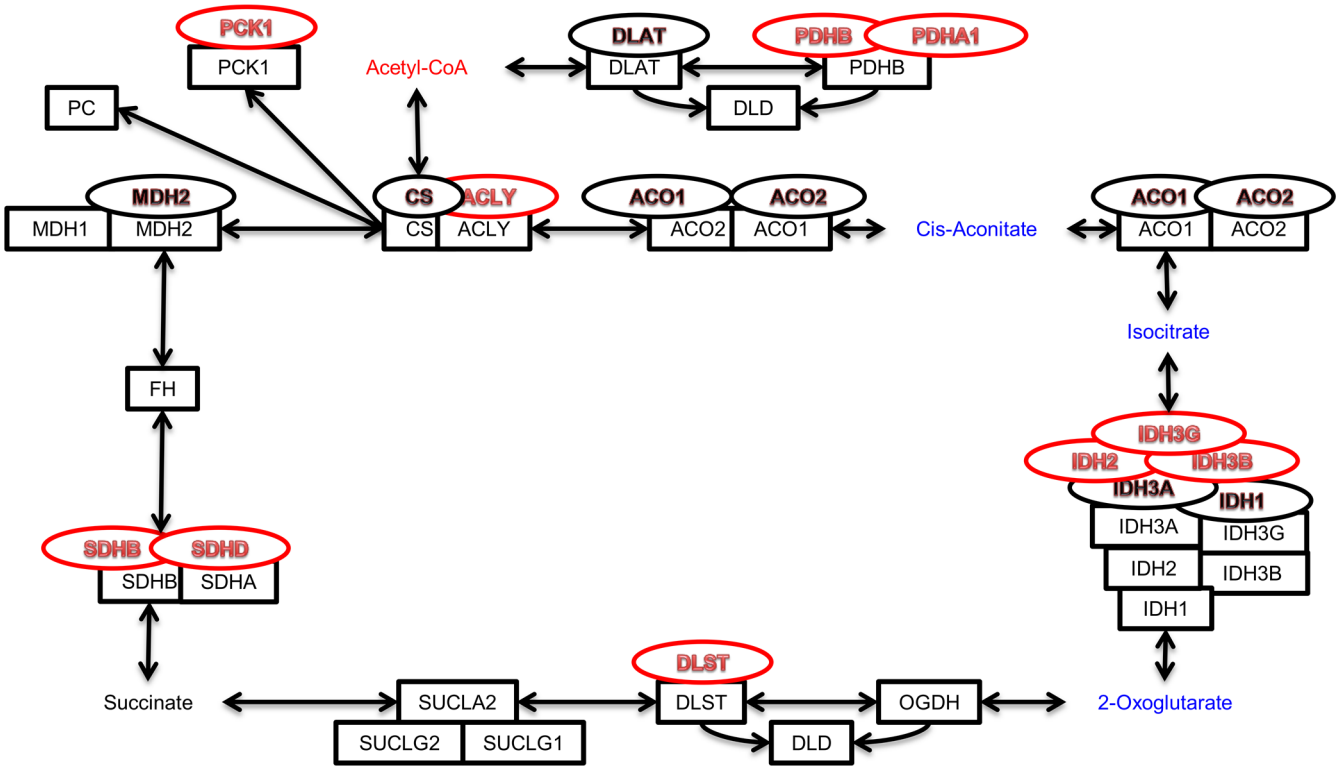

Figure 7. Simplified TCA cycle featuring transcriptomics, proteomics, and metabolomics regulations of LFD versus HFD in white adipose tissue, according to KEGG nomenclature. Transcriptomics data are presented as ovals, proteomics data as rectangles, metabolites by name. Regulation is color coded in which red stands for up regulated, blue for down regulated, and black for unregulated. For transcriptomics and proteomics, ≥ 1.5-fold changes were regarded as regulated, and for metabolomics, ≥ 2-fold changes were regarded as regulated.

standard deviation of 0.122, the proteome had the next largest at 0.329, and the metabolome had the largest standard deviation of 0.535—all of which were based on log10 fold ratios. Comparing the expression levels of individual RNAs with their corresponding proteins, the mean correlation coefficient was 65% from all analyzed tissues and treatments (Supporting Information, Figure 1A,C), suggesting rather slight correlation between gene and corresponding protein expression. However, regulation on the pathway level showed a higher mean correlation coefficient of 73% over all analyzed tissues and treatments (Supporting Information, Figure 1B,D).

Varying or even contradicting data correlations between transcriptome and proteome have already been observed by different research groups.[39,40] Weak data correlation can be explained in part by molecular events such as alternative splicing, assembly into complexes, post transcriptional modifications, secretion, and different half-life times of RNAs and proteins, among others. In general, our analyses indicated improved correlation of genes and proteins on the pathway level, indicating that physiological plasticity to counteract chronic metabolic stress in peripheral tissues such as WAT and liver may result from the concerted action of gene and protein ensembles, rather than from the isolated action of single players.

Network Analysis

Using our protein expression data sets, we analyzed protein networks to infer and characterize hub proteins that may exert major functions during HFD and drug treatment with RGZ. Only the proteins which were down regulated in LFD/HFD and RGZ-HFD/HFD in WAT generated large networks (Figure 5), in contrast to liver tissue. The KEGG pathway affiliation of these networks was examined and revealed that the networks belong to energy metabolism (e.g., OXPHOS, TCA cycle, and branched chain amino acids (BCAA)). The network similarity between LFD/HFD and RGZ-HFD/HFD in WAT (Figure 5) shows that the drug treatment by RGZ puts the HFD condition in part back to a LFD-like condition. This was confirmed by a direct network comparison of LFD versus RGZ-HFD, resulting in a neutralization of the TCA and OXPHOS networks (Supporting Information, Figure 2).

To identify the main important proteins within the discussed networks, we used the Cytoscape plug in "network analyzer" and a robustness test to identify the hubs. The main hub protein (in terms of centrality and robustness) in both networks was succinate dehydrogenase iron−sulfur subunit (SDHB; 2-fold up regulated due to HFD, 1.5-fold up regulated due to RGZ treatment), part of the TCA cycle and respiratory chain. Furthermore, succinyl-CoA ligase subunit alpha (SUCLG1; 1.5 fold up regulated for HFD and for RGZ), catalyzing the ATP- or GTP-dependent ligation of succinate and CoA to form succinyl-CoA was a main hub (Table 2). This shows again the effectiveness of RGZ to turn HFD WAT into a LFD-like condition.

Integrating Transcriptomics, Proteomics, and Metabolomics Data

As discussed above, a number of genes, proteins, and metabolites were detected, which deserve further attention and in depth functional study and validation as potential biomarkers. On the other hand, it seems that the biological function of complex physiological processes in diet-induced insulin resistance and during drug treatment might be more adequately described on the pathways level rather than focusing

dx.doi.org/10.1021/pr5005828 | J. Proteome Res. XXXX, XXX, XXX−XXX

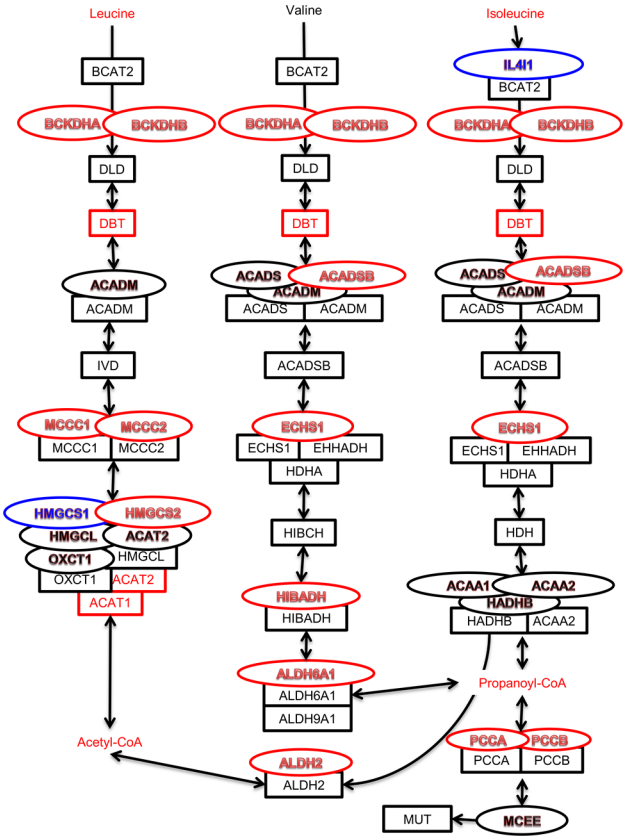

Figure 8. Simplified valine, leucine, and isoleucine degradation pathway featuring transcriptomics, proteomics, and metabolomics regulations of LFD versus HFD in white adipose tissue. Transcriptomics data are presented as ovals, proteomics data as rectangles, metabolites by name. Regulation is color coded in which red stands for up regulated, blue for down regulated, and black for unregulated. For transcriptomics and proteomics, ≥ 1.5-fold changes were regarded as regulated, and for metabolomics, ≥ 2-fold changes were regarded as regulated.

excessively on individual molecules, thereby potentially loosing causative context.[2,3]

Clearly, as a result of current technical maturity and feasibility, RNA expression data are presently the most comprehensive and the most informative and include more than 10 000 detected genes, followed by the proteomics data sets with about 3500 detected proteins, and metabolites data sets containing few hundreds of molecules.

In order to combine and strengthen pathway analyses of these data sets, we applied integrated pathway enrichment analysis (IMPaLa),[28] as shown in Figure 6. Significant pathways and their log10 FDR values from all three omics data sets were integrated. As a result of HFD, mitochondrial energy metabolism and BCAA metabolism were the most significant deregulated pathways in WAT. Upon RGZ treatment, the PPAR signaling pathway was identified as deregulated, indicating a distinct effect of the PPARγ-targeting drug RGZ in WAT (Figure 6A). In liver (Figure 6B), we observed that oxidative phosphorylation and ribosomes were the most deregulated pathways in HFD mice. Notably, our integrated pathway analysis revealed that RGZ treatment did not show strong regulation in liver, consistent with the rather low abundance of PPARγ in this tissue. This analysis indicated high specificity of RGZ for PPARγ compared to PPARα, which is highly abundant in liver, or the ubiquitously expressed PPARβ/δ.

For a more detailed pathway analysis of transcripts, proteins, and metabolites, we picked the citric acid cycle (TCA) as a strongly regulated pathway between HFD/LFD condition in WAT (Figure 7). More than half of the detected RNAs were at least 1.5-fold up regulated, whereas all detected proteins in this pathway were not significantly regulated on the basis of individual protein ratios, although the whole protein pathway was significantly up regulated (see Supporting Information, Figure 1B). Notably, although RNA and protein levels were up regulated, metabolites within the TCA cycle were down regulated, except incoming acetyl-CoA, which was 2-fold up regulated. This result shows fine-tuned regulations at the three investigated interconnected biological levels: Up regulated levels of RNAs or proteins do not necessarily mean that there are more metabolites present, but may rather indicate compensatory relative effects to regain metabolic homeostasis.

We further analyzed the valine, leucine, and isoleucine degradation pathway in more detail between LFD/HFD condition in WAT (Figure 8).

We observed a significant up regulation on the BCAA pathway level for RNA and protein data sets (Supporting Information, Figure 1B). Notably, a recent study of morbidly obese subjects with type 2 diabetes suggested that the reduction in blood of BCAA resulting from gastric bypass surgery may be associated with improvement in blood sugar regulation.[41] Our data indicate that increased amounts of BCAA induce an increasing expression of genes and proteins required for degradation of BCAA. Furthermore, the up regulation of this pathway could be a compensatory reaction for the down regulated energy metabolism in the HFD state, as this amino acid breakdown generates acyl-CoA derivatives, which can enter the TCA cycle.

CONCLUSIONS AND OUTLOOK

To the best of our knowledge, this is one of the first studies integrating transcriptomics, proteomics, and metabolomics data sets to analyze in mammalian tissues disease states and medical intervention in a preclinical setting.

Many diabetes-indicative plasma biomarkers such as BCAAs and acylcarnitines could be found in this study in the context of WAT and liver, corroborating recent findings that were exclusively based on analyzing plasma.[11,12,42] As described above, we further detected a number of RNA-, protein-, and metabolite-based biomarker candidates. In particular, we observed up regulation of HFD responsive proteins of TCA cycle and OXPHOS such as SDHB and SUCLG1 in WAT and down regulation of HFD responsive proteins involved in vitamin B metabolism such as PDXDC1 and DHFR in liver. Consistently, we detected down regulation of metabolites from the vitamin B group. Moreover, we found the sphingosine/sphingosine 1-phosphate pair as a potential marker for xenobiotic effects in liver. Using network and pathway analyses, we could demonstrate in major pathways (TCA cycle, OXPHOS, and BCAA metabolism) the adverse effects of HFD and specific restoring effects of rosiglitazone treatment in WAT. Identified proteins and metabolites need to be further validated, either as single markers or as marker sets for targeted and integrated genomics, proteomics, and metabolomics approaches.

dx.doi.org/10.1021/pr5005828 | J. Proteome Res. XXXX, XXX, XXX−XXX

■ ASSOCIATED CONTENT

Supporting Information

Detailed information on regulated RNA, proteins, and metabolites; correlation between gene and protein expression; network of down regulated proteins; gradient conditions for metabolite LC separation; ratios of metabolites; metabolite profiles of acylcarnitines. This material is available free of charge via the Internet at http://pubs.acs.org

■ AUTHOR INFORMATION

Corresponding Author

*E-mail: sauer@molgen.mpg.de. Fax: +49-30-84131960. Phone: +49-30-84131661.

Notes

The authors declare no competing financial interest.

■ ACKNOWLEDGMENTS

We thank Uli Stelzl for valuable input for testing network robustness and Beata Lukazewska for assistance during metabolite isolation and MS analysis. Our work was supported by the German Ministry for Education and Research (BMBF, grant number 0315082/01EA1303), the European Union (FP7/2007−2013), under grant agreement no. 262055 (ESGI)), and the Max Planck Society.

■ ABBREVIATIONS

DIO, diet-induced obesity; HFD, high fat diet; LFD, low fat diet; WAT, white adipose tissue; GSEA, gene set enrichment analysis; RGZ, rosiglitazone; MRM, multiple reaction monitoring

■ REFERENCES

(1) Ezzati, M.; Riboli, E. Can noncommunicable diseases be prevented? Lessons from studies of populations and individuals. *Science* **2012**, *337* (6101), 1482−1487.

(2) Barabasi, A. L. Network medicine–from obesity to the "diseasome". *N. Engl. J. Med.* **2007**, *357* (4), 404−407.

(3) Goh, K. I.; Cusick, M. E.; Valle, D.; Childs, B.; Vidal, M.; Barabasi, A. L. The human disease network. *Proc. Natl. Acad. Sci. U.S.A.* **2007**, *104* (21), 8685−8690.

(4) Sanchez, J. C.; Converset, V.; Nolan, A.; Schmid, G.; Wang, S.; Heller, M.; Sennitt, M. V.; Hochstrasser, D. F.; Cawthorne, M. A. Effect of rosiglitazone on the differential expression of diabetes-associated proteins in pancreatic islets of C57Bl/6 lep/lep mice. *Mol. Cell. Proteomics* **2002**, *1* (7), 509−516.

(5) Papale, M.; Di Paolo, S.; Vocino, G.; Rocchetti, M. T.; Gesualdo, L. Proteomics and diabetic nephropathy: what have we learned from a decade of clinical proteomics studies? *J. Nephrol.* **2014**, *27* (3), 221−228.

(6) Yang, M.; Liu, W.; Wang, C. Y.; Liu, T.; Zhou, F.; Tao, J.; Wang, Y.; Li, M. T. Proteomic analysis of differential protein expression in early process of pancreatic regeneration in pancreatectomized rats. *Acta. Pharmacol. Sin.* **2006**, *27* (5), 568−578.

(7) Sanchez, J. C.; Chiappe, D.; Converset, V.; Hoogland, C.; Binz, P. A.; Paesano, S.; Appel, R. D.; Wang, S.; Sennitt, M.; Nolan, A.; Cawthorne, M. A.; Hochstrasser, D. F. The mouse SWISS-2D PAGE database: a tool for proteomics study of diabetes and obesity. *Proteomics* **2001**, *1* (1), 136−163.

(8) Hittel, D. S.; Hathout, Y.; Hoffman, E. P.; Houmard, J. A. Proteome analysis of skeletal muscle from obese and morbidly obese women. *Diabetes* **2005**, *54* (5), 1283−1288.

(9) Guo, Y.; Darshi, M.; Ma, Y.; Perkins, G. A.; Shen, Z.; Haushalter, K. J.; Saito, R.; Chen, A.; Lee, Y. S.; Patel, H. H.; Briggs, S. P.; Ellisman, M. H.; Olefsky, J. M.; Taylor, S. S. Quantitative proteomic and functional analysis of liver mitochondria from high fat diet (HFD) diabetic mice. *Mol. Cell. Proteomics* **2013**, *12* (12), 3744−3758.

(10) Edvardsson, U.; von Lowenhielm, H. B.; Panfilov, O.; Nystrom, A. C.; Nilsson, F.; Dahllof, B. Hepatic protein expression of lean mice and obese diabetic mice treated with peroxisome proliferator-activated receptor activators. *Proteomics* **2003**, *3* (4), 468−478.

(11) Floegel, A.; Stefan, N.; Yu, Z.; Muhlenbruch, K.; Drogan, D.; Joost, H. G.; Fritsche, A.; Haring, H. U.; Hrabe de Angelis, M.; Peters, A.; Roden, M.; Prehn, C.; Wang-Sattler, R.; Illig, T.; Schulze, M. B.; Adamski, J.; Boeing, H.; Pischon, T. Identification of serum metabolites associated with risk of type 2 diabetes using a targeted metabolomic approach. *Diabetes* **2013**, *62* (2), 639−648.

(12) Wang, T. J.; Larson, M. G.; Vasan, R. S.; Cheng, S.; Rhee, E. P.; McCabe, E.; Lewis, G. D.; Fox, C. S.; Jacques, P. F.; Fernandez, C.; O'Donnell, C. J.; Carr, S. A.; Mootha, V. K.; Florez, J. C.; Souza, A.; Melander, O.; Clish, C. B.; Gerszten, R. E. Metabolite profiles and the risk of developing diabetes. *Nat. Med.* **2011**, *17* (4), 448−453.

(13) Rull, A.; Geeraert, B.; Aragones, G.; Beltran-Debon, R.; Rodriguez-Gallego, E.; Garcia-Heredia, A.; Pedro-Botet, J.; Joven, J.; Holvoet, P.; Camps, J. Rosiglitazone and fenofibrate exacerbate liver steatosis in a mouse model of obesity and hyperlipidemia. A transcriptomic and metabolomic study. *J. Proteome Res.* **2014**, *13* (3), 1731−1743.

(14) Weidner, C.; Wowro, S. J.; Freiwald, A.; Kawamoto, K.; Witzke, A.; Kliem, M.; Siems, K.; Muller-Kuhrt, L.; Schroeder, F. C.; Sauer, S. Amorfrutin B is an efficient natural peroxisome proliferator-activated receptor gamma (PPARgamma) agonist with potent glucose-lowering properties. *Diabetologia* **2013**, *56* (8), 1802−1812.

(15) Weidner, C.; de Groot, J. C.; Prasad, A.; Freiwald, A.; Quedenau, C.; Kliem, M.; Witzke, A.; Kodelja, V.; Han, C. T.; Giegold, S.; Baumann, M.; Klebl, B.; Siems, K.; Muller-Kuhrt, L.; Schurmann, A.; Schuler, R.; Pfeiffer, A. F.; Schroeder, F. C.; Bussow, K.; Sauer, S. Amorfrutins are potent antidiabetic dietary natural products. *Proc. Natl. Acad. Sci. U.S.A.* **2012**, *109* (19), 7257−7262.

(16) Meierhofer, D.; Weidner, C.; Hartmann, L.; Mayr, J. A.; Han, C. T.; Schroeder, F. C.; Sauer, S. Protein sets define disease states and predict in vivo effects of drug treatment. *Mol. Cell. Proteomics* **2013**, *12* (7), 1965−1979.

(17) Lehmann, J. M.; Moore, L. B.; Smith-Oliver, T. A.; Wilkison, W. O.; Willson, T. M.; Kliewer, S. A. An antidiabetic thiazolidinedione is a high affinity ligand for peroxisome proliferator-activated receptor gamma (PPAR gamma). *J. Biol. Chem.* **1995**, *270* (22), 12953−12956.

(18) Chao, L.; Marcus-Samuels, B.; Mason, M. M.; Moitra, J.; Vinson, C.; Arioglu, E.; Gavrilova, O.; Reitman, M. L. Adipose tissue is required for the antidiabetic, but not for the hypolipidemic, effect of thiazolidinediones. *J. Clin. Invest.* **2000**, *106* (10), 1221−1228.

(19) Tschop, M. H.; Speakman, J. R.; Arch, J. R.; Auwerx, J.; Bruning, J. C.; Chan, L.; Eckel, R. H.; Farese, R. V., Jr.; Galgani, J. E.; Hambly, C.; Herman, M. A.; Horvath, T. L.; Kahn, B. B.; Kozma, S. C.; Maratos-Flier, E.; Muller, T. D.; Munzberg, H.; Pfluger, P. T.; Plum, L.; Reitman, M. L.; Rahmouni, K.; Shulman, G. I.; Thomas, G.; Kahn, C. R.; Ravussin, E. A guide to analysis of mouse energy metabolism. *Nat. Methods* **2012**, *9* (1), 57−63.

(20) Cox, J.; Mann, M. 1D and 2D annotation enrichment: a statistical method integrating quantitative proteomics with complementary high-throughput data. *BMC Bioinf.* **2012**, *13* (Suppl 16), S12.

(21) Wu, H.; Southam, A. D.; Hines, A.; Viant, M. R. High-throughput tissue extraction protocol for NMR- and MS-based metabolomics. *Anal. Biochem.* **2008**, *372* (2), 204−212.

(22) Subramanian, A.; Tamayo, P.; Mootha, V. K.; Mukherjee, S.; Ebert, B. L.; Gillette, M. A.; Paulovich, A.; Pomeroy, S. L.; Golub, T. R.; Lander, E. S.; Mesirov, J. P. Gene set enrichment analysis: a knowledge-based approach for interpreting genome-wide expression profiles. *Proc. Natl. Acad. Sci. U.S.A.* **2005**, *102* (43), 15545−15550.

(23) Battke, F.; Symons, S.; Nieselt, K. Mayday–integrative analytics for expression data. *BMC Bioinf.* **2010**, *11*, 121.

(24) Franceschini, A.; Szklarczyk, D.; Frankild, S.; Kuhn, M.; Simonovic, M.; Roth, A.; Lin, J.; Minguez, P.; Bork, P.; von Mering, C.; Jensen, L. J. STRING v9.1: protein-protein interaction networks, with

increased coverage and integration. *Nucleic Acids Res.* **2013**, *41* (Database issue), D808−D815.
(25) Cline, M. S.; Smoot, M.; Cerami, E.; Kuchinsky, A.; Landys, N.; Workman, C.; Christmas, R.; Avila-Campilo, I.; Creech, M.; Gross, B.; Hanspers, K.; Isserlin, R.; Kelley, R.; Killcoyne, S.; Lotia, S.; Maere, S.; Morris, J.; Ono, K.; Pavlovic, V.; Pico, A. R.; Vailaya, A.; Wang, P. L.; Adler, A.; Conklin, B. R.; Hood, L.; Kuiper, M.; Sander, C.; Schmulevich, I.; Schwikowski, B.; Warner, G. J.; Ideker, T.; Bader, G. D. Integration of biological networks and gene expression data using Cytoscape. *Nat. Protoc.* **2007**, *2* (10), 2366−2382.
(26) Assenov, Y.; Ramirez, F.; Schelhorn, S. E.; Lengauer, T.; Albrecht, M. Computing topological parameters of biological networks. *Bioinformatics* **2008**, *24* (2), 282−284.
(27) Nair, J.; Ghatge, M.; Kakkar, V. V.; Shanker, J. Network analysis of inflammatory genes and their transcriptional regulators in coronary artery disease. *PLoS One* **2014**, *9* (4), e94328.
(28) Kamburov, A.; Cavill, R.; Ebbels, T. M.; Herwig, R.; Keun, H. C. Integrated pathway-level analysis of transcriptomics and metabolomics data with IMPaLA. *Bioinformatics* **2011**, *27* (20), 2917−2918.
(29) Nakatani, S.; Kakehashi, A.; Ishimura, E.; Yamano, S.; Mori, K.; Wei, M.; Inaba, M.; Wanibuchi, H. Targeted proteomics of isolated glomeruli from the kidneys of diabetic rats: sorbin and SH3 domain containing 2 is a novel protein associated with diabetic nephropathy. *Exp. Diabetes Res.* **2011**, *2011*, 979354.
(30) Cohadon, F.; Rigoulet, M.; Guerin, B.; Vandendriessche, M. [Vasogenic cerebral oedema. Changes in membrane ATPases. Correction by a phospholipid precursor (author's transl)]. *Nouv. Presse Med.* **1979**, *8* (19), 1589−1591.
(31) Maceyka, M.; Payne, S. G.; Milstien, S.; Spiegel, S. Sphingosine kinase, sphingosine-1-phosphate, and apoptosis. *Biochim. Biophys. Acta* **2002**, *1585* (2−3), 193−201.
(32) Floyd, J. S.; Barbehenn, E.; Lurie, P.; Wolfe, S. M. Case series of liver failure associated with rosiglitazone and pioglitazone. *Pharmacoepidemiol. Drug Saf.* **2009**, *18* (12), 1238−1243.
(33) Chen, J.; Gall, M. A.; Yokoyama, H.; Jensen, J. S.; Deckert, M.; Parving, H. H. Raised serum sialic acid concentration in NIDDM patients with and without diabetic nephropathy. *Diabetes Care* **1996**, *19* (2), 130−134.
(34) Scriver, C. R.; Hutchison, J. H. The vitamin B6 deficiency syndrome in human infancy: biochemical and clinical observations. *Pediatrics* **1963**, *31*, 240−250.
(35) Rutkowsky, J. M.; Knotts, T. A.; Ono-Moore, K. D.; McCoin, C. S.; Huang, S.; Schneider, D.; Singh, S.; Adams, S. H.; Hwang, D. H. Acylcarnitines Activate Pro-Inflammatory Signaling Pathways. *Am. J. Physiol. Endocrinol. Metab.* **2014**, *306* (12), E1378−E1387.
(36) Adams, S. H.; Hoppel, C. L.; Lok, K. H.; Zhao, L.; Wong, S. W.; Minkler, P. E.; Hwang, D. H.; Newman, J. W.; Garvey, W. T. Plasma acylcarnitine profiles suggest incomplete long-chain fatty acid beta-oxidation and altered tricarboxylic acid cycle activity in type 2 diabetic African-American women. *J. Nutr.* **2009**, *139* (6), 1073−1081.
(37) Schooneman, M. G.; Vaz, F. M.; Houten, S. M.; Soeters, M. R. Acylcarnitines: reflecting or inflicting insulin resistance? *Diabetes* **2013**, *62* (1), 1−8.
(38) Mihalik, S. J.; Goodpaster, B. H.; Kelley, D. E.; Chace, D. H.; Vockley, J.; Toledo, F. G.; DeLany, J. P. Increased levels of plasma acylcarnitines in obesity and type 2 diabetes and identification of a marker of glucolipotoxicity. *Obesity (Silver Spring)* **2010**, *18* (9), 1695−1700.
(39) Gygi, S. P.; Rochon, Y.; Franza, B. R.; Aebersold, R. Correlation between protein and mRNA abundance in yeast. *Mol. Cell. Biol.* **1999**, *19* (3), 1720−1730.
(40) Futcher, B.; Latter, G. I.; Monardo, P.; McLaughlin, C. S.; Garrels, J. I. A sampling of the yeast proteome. *Mol. Cell. Biol.* **1999**, *19* (11), 7357−7368.
(41) Laferrere, B.; Reilly, D.; Arias, S.; Swerdlow, N.; Gorroochurn, P.; Bawa, B.; Bose, M.; Teixeira, J.; Stevens, R. D.; Wenner, B. R.; Bain, J. R.; Muehlbauer, M. J.; Haqq, A.; Lien, L.; Shah, S. H.; Svetkey, L. P.; Newgard, C. B. Differential metabolic impact of gastric bypass surgery versus dietary intervention in obese diabetic subjects despite identical weight loss. *Sci. Transl. Med.* **2011**, *3* (80), 80re2.
(42) Xie, G.; Ma, X.; Zhao, A.; Wang, C.; Zhang, Y.; Nieman, D.; Nicholson, J. K.; Jia, W.; Bao, Y.; Jia, W. The metabolite profiles of the obese population are gender-dependent. *J. Proteome Res.* **2014**, *13* (9), 4062−4073.